

Numerical Study of Wind-Tunnel Walls Effects on Transonic Airfoil Flow

Andrey Garbaruk,^{*} Mikhail Shur,[†] and Mikhail Strelets[‡]

St. Petersburg State Technical University, 195251, St. Petersburg, Russia

and

Philippe R. Spalart[§]

The Boeing Company, Seattle, Washington 98124-2207

The flow past the Royal Aircraft Establishment (RAE) 2822 airfoil is studied by three-dimensional computational fluid dynamics (CFD), which includes the viscous side walls of the wind-tunnel test, with an aspect ratio of 3. Three turbulence models, two aspect ratios, and several grids are used, as well as two treatments of the floor and ceiling (neither one actually representing slotted surfaces) and small Mach number and incidence adjustments. The results deviate from two-dimensional results sufficiently to revisit the quantitative conclusions and the ranking of turbulence models that were made from two-dimensional CFD in the 1980s and 1990s. However, contrary to our hopes, the three-dimensional effects fail to improve the pressure recovery after shock-induced separation in the more difficult case 10, so that all of the turbulence models we tried still fail to match measurements by modern standards, even with Mach number and angle-of-attack adjustments. The unseparated case 6 produces very similar trends. With present levels of computer power, tests with fully documented three-dimensional solid-wall boundary conditions appear most desirable, but axisymmetric test cases can already be quite useful.

Introduction

THE dominant features of the flow over a transonic airfoil nearing buffet are a strong adverse pressure gradient, shock/boundary-layer interaction, and separation downstream of the shock. That makes an accurate prediction of the major characteristics of such flows (shock location, extent of the separation zone, and pressure recovery downstream of the shock and in the trailing-edge zone) a severe challenge for computational fluid dynamics (CFD) codes and turbulence models. These characteristics control lift, pitching moment, and hinge moments on a wing in crucial flight conditions. For this reason, experimental data on transonic airfoils and, first of all, those on the Royal Aircraft Establishment (RAE) 2822 airfoil,¹ which are considered the most complete and reliable, are widely used for evaluation of turbulence-model capabilities. (See, for instance, Refs. 2–5, as well as the EC Project⁶ directed at a knowledge base on experiments, test data, sample computations, procedures, and guidelines relating to the industrial challenges in fluid mechanics.) However, some methodological issues associated with the interpretation of the data remain unresolved.

The conventional practice in CFD studies of the RAE 2822 flow has been to use the two-dimensional Reynolds-averaged Navier–Stokes (RANS) equations, the experiments having been designed to provide two-dimensional flow to the best possible degree. Still, to account for differences between “free air” CFD and the real wind-tunnel environment and, in particular, the slotted floor and ceiling, numerous correction procedures have been used. One procedure consists of adjusting the airfoil angle of attack so that the predicted lift coefficient is equal to the experimental one, or so that the preshock pressure level matches. Then, a turbulence model is evaluated by the level of disagreement between the computed and

measured drag coefficients and other flow quantities at that adjusted angle of attack. At least with some turbulence models, including the Spalart–Allmaras model² (S-A) and the $k-\omega$ model of Menter⁷ (M-SST), this procedure provides quite an acceptable accuracy for shock position and airfoil drag (see, for example, Refs. 2 and 4), although a very noticeable discrepancy, especially in the region downstream of the shock of case 10, still exists. It has commonly been attributed to the turbulence models’ deficiencies, but many models have now been tried without success, including higher-order models, compared with S-A and M-SST.

The two-dimensional character of the experimental flow is not demonstrated beyond doubt by direct measurements, and the aspect ratio of the wing, namely 3, is not very large, which could be the source of the observed discrepancy. Also, the slotted floor and ceiling of the test section in the experiments, although they effectively weaken the blockage effect, are unfortunate from a CFD point of view because we have no simple boundary conditions that duplicate them. In addition, they could interact with the side-wall boundary layers in ways that defeat any simple correction procedure. Besides, the plenum chamber that is behind the slots is not known in any detail.

Therefore, until now, it has not been clear whether a comparison of conventional two-dimensional CFD with the RAE 2822 data provides an objective information on the real capabilities of turbulence models or, as stated in Ref. 8, two-dimensional tests may not be definitive as applied to transonic airfoil flows. Our expectations have risen since the test was conducted. That provides a strong motivation for more careful studies of the RAE 2822 flow and, particularly, for a direct evaluation of the three-dimensional effects in the experiments.

In this paper, we present the results of such a study, which is quite similar to that of Jiang⁹ for another test. First, we briefly discuss the problem statement, the numerical algorithm used in the computations, and the complete design of the study. We then present and discuss the major findings.

Problem Statement, Numerical Method, and Design of the Study

A summary of the computed cases is presented in Table 1. The computations were performed in the framework of the three-dimensional RANS equations, mostly with the use of the S-A turbulence model. Along with that, to estimate the model sensitivity, a

Received 29 July 2002; revision received 31 January 2003; accepted for publication 31 January 2003. Copyright © 2003 by the American Institute of Aeronautics and Astronautics, Inc. All rights reserved. Copies of this paper may be made for personal or internal use, on condition that the copier pay the \$10.00 per-copy fee to the Copyright Clearance Center, Inc., 222 Rosewood Drive, Danvers, MA 01923; include the code 0001-1452/03 \$10.00 in correspondence with the CCC.

^{*}Associate Professor, Hydroaerodynamics Department.

[†]Associate Professor, Hydroaerodynamics Department. Member AIAA.

[‡]Professor, Hydroaerodynamics Department.

[§]Technical Fellow, Commercial Airplanes.

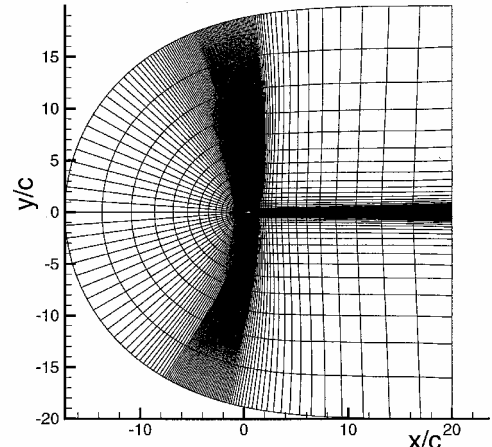
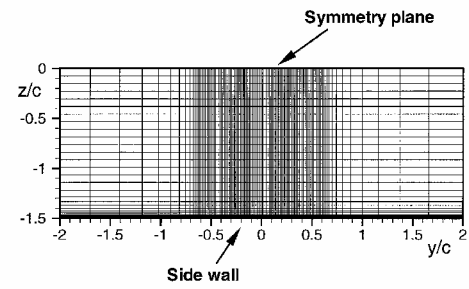
Table 1 List of cases computed for RAE 2822

| Number | Two-dimensional/ Three-dimensional | Side walls | Floor and ceiling | δ_{BL} | Model | Grid | α | M | C_l | C_d |
|----------------|---------------------------------------|---------------|----------------------|---------------|-------|-----------------------------------|----------|-------|-------|--------|
| <i>Case 10</i> | | | | | | | | | | |
| Experiment | | Yes | Slots | 0.075 | — | — | 3.19 | 0.75 | 0.743 | 0.0242 |
| 1 | Two-dimensional | No | No | | S-A | 193 × 65 | 3.19 | 0.75 | 0.762 | 0.0309 |
| 2 | Two-dimensional | No | No | | SARC | 193 × 65 | 3.19 | 0.75 | 0.742 | 0.0297 |
| 3 | Two-dimensional | No | No | | MSST | 193 × 65 | 3.19 | 0.75 | 0.733 | 0.0289 |
| 4 | Two-dimensional | No | No | | S-A | 193 × 65 | 2.57 | 0.75 | 0.720 | 0.0247 |
| 5 | Two-dimensional | No | No | | S-A | 193 × 65 | 3.50 | 0.75 | 0.774 | 0.0341 |
| 6 | Two-dimensional | No | No | | S-A | 193 × 65 | 3.19 | 0.73 | 0.837 | 0.0231 |
| 7 | Two-dimensional | No | No | | S-A | 193 × 65 | 3.19 | 0.77 | 0.654 | 0.0365 |
| 8 | Two-dimensional | No | No | | S-A | 385 × 65 | 3.19 | 0.75 | 0.754 | 0.0302 |
| 9 | Two-dimensional | No | No | | S-A | 385 × 97 | 3.19 | 0.75 | 0.777 | 0.0316 |
| 10 | Two-dimensional | No | Yes | | S-A | (176 × 53) + (81 × 81) | 3.19 | 0.75 | 0.682 | 0.0393 |
| 11 | Three-dimensional | Yes | No | 0.075 | S-A | 193 × 65 × 53 | 3.19 | 0.75 | 0.654 | 0.0253 |
| 12 | Three-dimensional | Yes | No | 0.075 | SARC | 193 × 65 × 53 | 3.19 | 0.75 | 0.652 | 0.0251 |
| 13 | Three-dimensional | Yes | No | 0.075 | MSST | 193 × 65 × 53 | 3.19 | 0.75 | 0.602 | 0.0245 |
| 14 | Three-dimensional | Yes | No | 0.075 | S-A | 193 × 65 × 53 | 2.57 | 0.75 | 0.587 | 0.0205 |
| 15 | Three-dimensional | Yes | No | 0.075 | S-A | 193 × 65 × 53 | 3.50 | 0.75 | 0.687 | 0.0281 |
| 16 | Three-dimensional | Yes | No | 0.075 | S-A | 193 × 65 × 53 | 3.19 | 0.73 | 0.657 | 0.0221 |
| 17 | Three-dimensional | Yes | No | 0.075 | S-A | 193 × 65 × 53 | 3.19 | 0.77 | 0.643 | 0.0322 |
| 18 | Three-dimensional | Yes | No | 0.063 | S-A | 193 × 65 × 53 | 3.19 | 0.75 | 0.658 | 0.0258 |
| 19 | Three-dimensional | Yes | No | 0.075 | S-A | 193 × 65 × 69 | 3.19 | 0.75 | 0.652 | 0.0254 |
| 20 | Three-dimensional | Yes | Yes | 0.075 | S-A | (176 × 53 × 53) + (112 × 45 × 53) | 3.19 | 0.75 | 0.702 | 0.0314 |
| <i>Case 6</i> | | | | | | | | | | |
| Experiment | | Yes | Slots | 0.075 | — | — | 2.92 | 0.725 | 0.743 | 0.0127 |
| 21 | Two-dimensional | No | No | | S-A | 193 × 65 | 2.92 | 0.725 | 0.806 | 0.0177 |
| 22 | Two-dimensional | No | No | | S-A | 193 × 65 | 2.50 | 0.725 | 0.739 | 0.0144 |
| 23 | Two-dimensional | No | No | | S-A | 193 × 65 | 3.40 | 0.725 | 0.868 | 0.0236 |
| 24 | Two-dimensional | No | No | | S-A | 193 × 65 | 2.92 | 0.71 | 0.796 | 0.0134 |
| 25 | Two-dimensional | No | No | | S-A | 193 × 65 | 2.92 | 0.74 | 0.791 | 0.0243 |
| 26 | Three-dimensional | Yes | No | 0.075 | S-A | 193 × 65 × 53 | 2.92 | 0.725 | 0.630 | 0.0198 |
| 27 | Three-dimensional | Yes | No | 0.075 | S-A | 193 × 65 × 53 | 2.50 | 0.725 | 0.583 | 0.0174 |
| 28 | Three-dimensional | Yes | No | 0.075 | S-A | 193 × 65 × 53 | 3.40 | 0.725 | 0.681 | 0.0229 |
| 29 | Three-dimensional | Yes | No | 0.075 | S-A | 193 × 65 × 53 | 2.92 | 0.71 | 0.628 | 0.0185 |
| 30 | Three-dimensional | Yes | No | 0.075 | S-A | 193 × 65 × 53 | 2.92 | 0.74 | 0.630 | 0.0213 |

baseline case (that with the experimental values of the angle of attack and Mach number) was computed with the use of two other models: the S-A model with the rotation/curvature correction¹⁰ (SARC model) and the M-SST model (runs 2 and 3 and 12 and 13 in Table 1, respectively).

For the solution of the governing equations, a multiblock structured flow solver was used based on the implicit upwind flux-difference splitting numerical scheme of Roe.¹¹ The inviscid fluxes were approximated with third-order accuracy and the viscous fluxes with second-order accuracy. The corresponding finite difference equations were solved by line (for two dimensions) and plane (for three dimensions) Gauss–Seidel relaxation for both the flowfield and turbulence-model equations.

In the first series of three-dimensional computations we have reproduced the experimental setup for the flow regime, case 10 from Ref. 1, but with account taken of the side walls of the test section only, not the slotted floor and ceiling (runs 11–19 in Table 1). The computational domain and grid used in that series are shown in Fig. 1. They assume symmetry of the flow in the spanwise direction z and include a symmetry plane ($z = 0$) and a side wall ($z/c = -1.5$), so that the size of the domain in the z direction is equal to one-half of the airfoil span, $1.5c$. The computational grid has two blocks. In the XY plane it has 193×65 nodes (128 of the 192 being on the airfoil) and is close to the grid used in the two-dimensional computations of the same flow in Ref. 4. As demonstrated there, it provides for a virtually grid-independent two-dimensional solution. (The same conclusion can be drawn on the basis of a comparison of runs 1 and 9.) In the spanwise direction, the grid has 53 nodes with clustering in the vicinity of the side wall ($z = -1.5$), so that the near-wall value of z^+ is not higher than 2, with another cluster in the vicinity of the airfoil ($y = 0$). A further refinement of this grid virtually does not affect the solution. (Compare runs 11 and 19.)

**a) Domain and grid in XY plane****b) Fragment of the grid in YZ plane****Fig. 1** Computational domain and grid used in the three-dimensional computations, with account taken of the side walls.

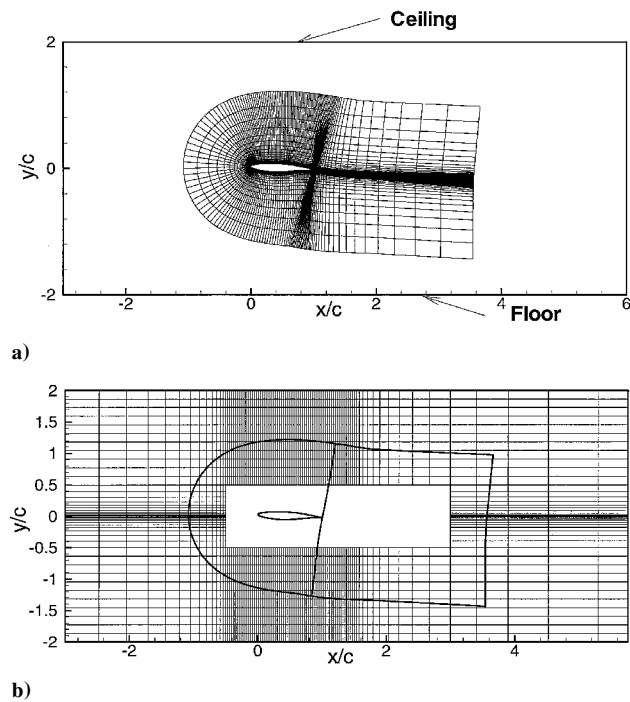


Fig. 2 Fragments of the three-block grid in the XY plane used in the three-dimensional computations, with account taken of the side walls, floor, and ceiling of the test section.

To estimate the effect of the airfoil aspect ratio, one run (run 11) has been repeated with aspect ratio 6, as opposed to 3 in the experiment.

As far as the freestream flow parameters (Mach number M and angle of attack α) are concerned, considering the uncertainty on their equivalent freestream values, we have varied both parameters in some range in the vicinity of their nominal values¹ ($M = 0.75$ and $\alpha = 3.19$ for case 10). In addition to that, some computations have been carried out for case 6 ($M = 0.725$, $\alpha = 2.92$ deg, runs 21–30).

Finally, to evaluate the maximum possible effect of the floor and ceiling of the test section, two more cases were computed. The first of them (run 10) is a two-dimensional flow with account taken of only the floor and ceiling. The second (run 20) is a three-dimensional flow with account taken of all four walls of the test section. In both cases, unlike the experimental setup with the slotted floor and ceiling, in the computations they are considered nonslotted free-slip boundaries; this will overstate the effect of these walls. The grid used in the four-wall computations is shown in Fig. 2; it has an additional block with $112 \times 45 \times 53$ nodes. The white area in Fig. 2b denotes the region that is cut out of the outer block and covered by the inner block only.

The boundary conditions used in the computations are as follows:

At the airfoil surface, we impose the conventional no-permeability and no-slip conditions for velocity components and zero pressure and temperature gradients. At the inlet and outlet of the domain, the boundary conditions are of the characteristic type, and at the symmetry plane ($z = 0$) symmetry conditions are used.

Finally, to reproduce the experimental thickness of the side-wall boundary layer at $x = 0$ (the coordinate of the airfoil leading edge), which was about $0.075c$, the no-slip boundary conditions at the side wall are imposed only over its part bounded by the grid line, which passes through $x = -4.3$ at $y = 0$. Outside that grid line, free-slip boundary conditions are used. This loosely approximates the effect of the wind-tunnel contraction. Recall that the side walls did not have any transpiration, in contrast to those considered by Jiang.⁹

Results and Discussion

Mechanism and Strength of the Side-Wall Effect

Figures 3 and 4a illustrate the unexpectedly strong effect of the side walls of the test section on the computed pressure coefficient

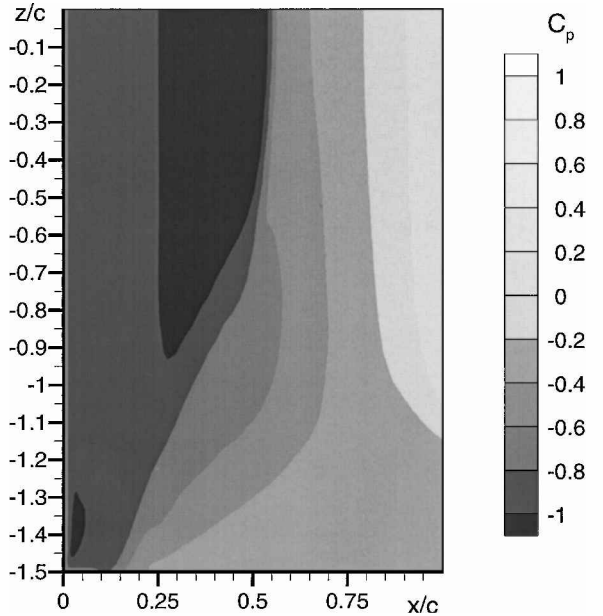


Fig. 3 Pressure coefficient distribution over the upper surface of the airfoil for run 11.

distribution over the airfoil surface. This is run 11, case 10, with the S-A model. The same trend is seen clearly in Fig. 5, which shows the Mach number fields at different span sections of the flow. A striking feature of the flow revealed by those Figs. 3–5 is that the side wall causes a strong alteration of the flow, not only in its close vicinity (which is quite natural), but up to the symmetry plane. For instance, the maximum value of the Mach number from the two-dimensional computation is equal to 1.36, whereas the maximum three-dimensional value at the symmetry plane is as low as 1.27. Also, as seen in Figs. 3–5, according to the three-dimensional RANS, an upper-surface shock forms only for $|z| \leq \approx 0.5c$. Outside of that region, the supersonic zone of the flow shrinks, and the streamwise pressure distribution becomes quite smooth. As a result, the skin-friction distribution over the airfoil also turns out to be qualitatively different from that observed in the two-dimensional computation. In particular, due to the weaker shock in the central part of the airfoil, no boundary-layer separation (negative skin friction) is observed there. On the other hand, near the side wall, the separation occurs at x about $0.2c$, that is, far upstream of the shock position at the airfoil symmetry plane. This is seen, for instance, in the skin-friction distribution at $z/c = -1.495$ (Fig. 4b).

The strong three dimensionality of the flow is seen also in Fig. 6, where we present transverse cuts of the pressure and streamwise velocity at $x/c = 0.4$, that is, somewhat upstream of the shock position. The pressure distribution over the upper surface of the airfoil is very nonuniform in the z direction. As a result, the spanwise velocity component (not shown) is also high (up to 0.15) and is directed toward the low-pressure region in the central part of the airfoil. The streamlines converge. Though the flow section is located quite a bit upstream of the shock, a separation zone is already quite noticeable. It shows up as a reverse flow in the corner, formed by the airfoil upper surface and the side wall. (Note a negative spot in the streamwise-velocity contours in Fig. 6b.) This early separation is very probably caused by the adverse pressure gradient in the boundary layer on the side wall. Note that the flow over the lower surface of the airfoil at $x/c = 0.4$ still remains virtually two-dimensional with only a relatively thin boundary layer at the side wall. This is consistent with the favorable pressure gradient near the lower surface.

Farther downstream, the trends just outlined continue and amplify to the trailing edge of the airfoil ($x/c = 1.0$). Namely, both pressure and Mach number fields remain strongly three-dimensional, with the high spanwise velocity region and the zone of reverse flow in the corner formed by the airfoil and side wall growing. Another feature

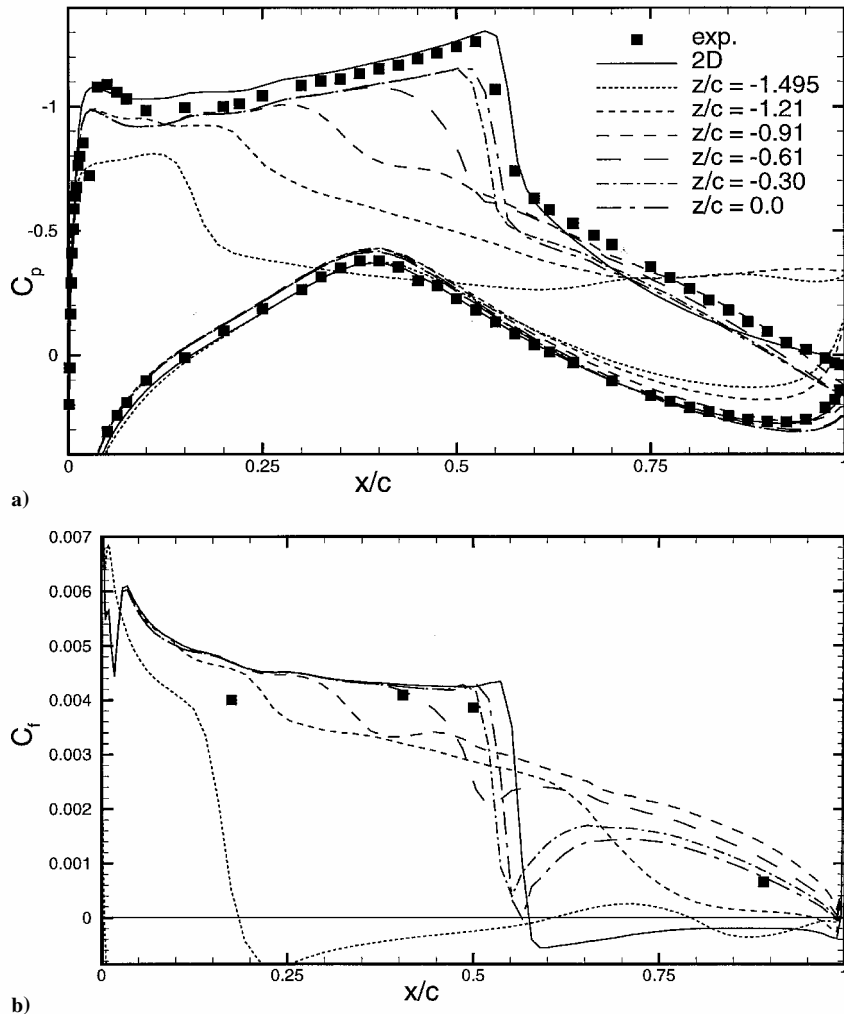


Fig. 4 Streamwise distributions at different span sections for run 11: a) pressure coefficient and b) friction coefficient.

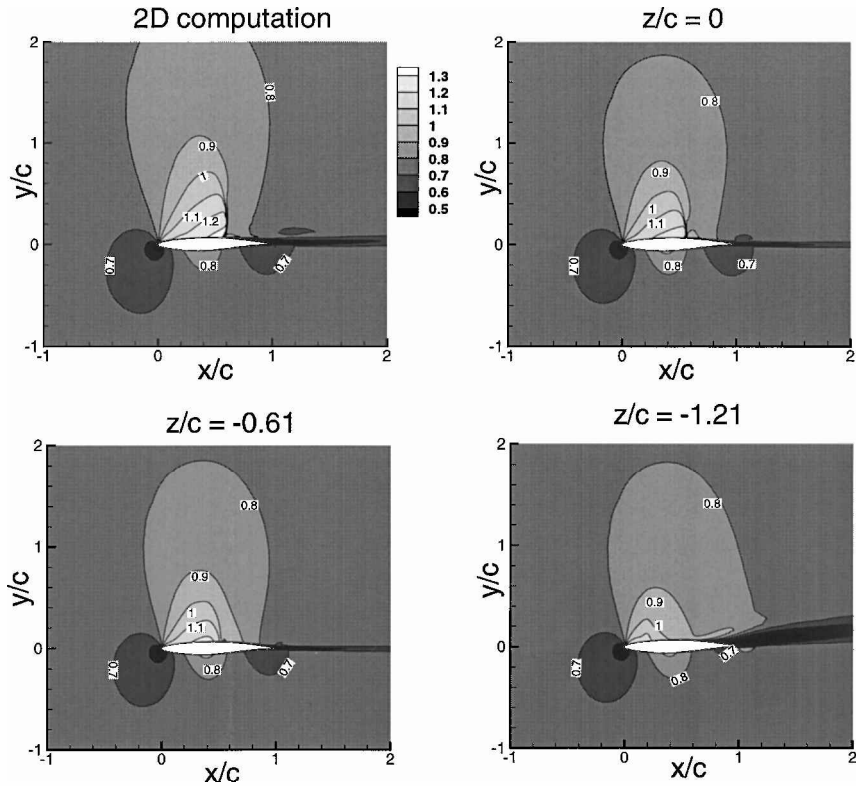


Fig. 5 Mach number fields at different spanwise sections for run 11 and run 1.

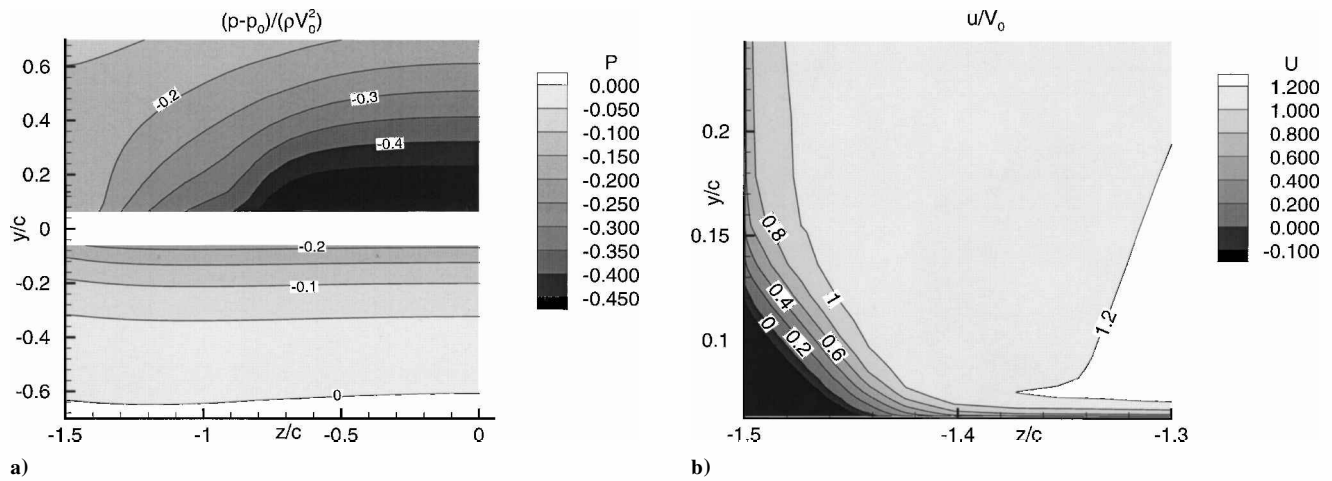


Fig. 6 Fragments of the YZ cuts of a) pressure and b) streamwise velocity component at $x/c = 0.4$ for run 11.

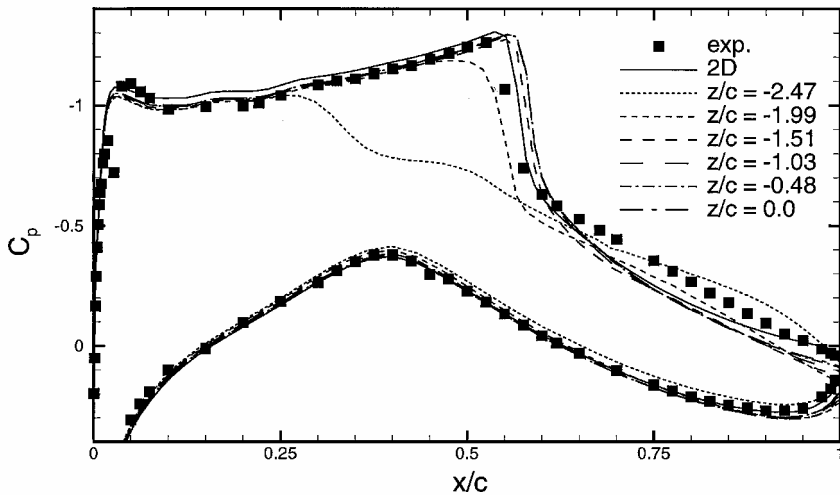


Fig. 7 Pressure coefficient streamwise distributions at different span sections for run 11 with doubled aspect ratio.

of the flowfield is the formation and gradual growth of a streamwise corner vortex. Beneath the airfoil, the flow remains virtually two-dimensional, almost down to $x/c = 1.0$, where some three dimensionality does show up due to interaction with the flow from the upper surface.

Farther downstream, in the airfoil wake region, the separation zone is gradually closing, and both the corner vortex and global flow three dimensionality are weakening. (For instance, the magnitude of the spanwise velocity at $x/c = 10$ is no higher than 0.05.) We do not focus on the wake, noting that turbulence models have not been deeply validated in such a region.

Thus, at the present aspect ratio and flow conditions, the interaction of the separated side-wall boundary layer with the flow over the upper surface of the airfoil causes a global change of the flow pattern. In the work of Jiang⁹ (also discussed by Spalart⁸) the effect of the side walls, even with boundary-layer suction, is qualitatively the same, which adds credibility to our results. Also, the admittedly modest spanwise-grid refinement we have performed does not result in any noticeable change of the solution. (Compare runs 11 and 19.) Finally, to make sure that the effect is not caused by some inconsistency in our three-dimensional problem statement, we have repeated run 11 with a doubled aspect ratio, $d = 6$ vs 3 in the experiment. As expected, the results of this computation at the symmetry plane of the airfoil turn out to be much closer to the two-dimensional prediction of the same flow than those with the baseline aspect ratio of 3. This is illustrated in Fig. 7 where we compare the pressure distribution over the airfoil at different span sections from the three-dimensional solution at $d = 6$ with the corresponding two-dimensional solution.

All of those observations seem quite sufficient to conclude that the unexpectedly strong effect of the side walls found in our computations of the airfoil with aspect ratio 3 is not caused by any numerical inconsistency and can be considered established.

As for the agreement between three-dimensional computations accounting for the side walls and the experimental data (the latter presented in Figs. 1–7 and Table 1), it turns out far from perfect, dashing hopes that the improved CFD setup would at last resolve the pressure discrepancy on case 10. The remaining candidates include a deficiency of the S-A turbulence model and the effect of the slotted floor and ceiling of the test section in the experiments. Though the authors of the experiment deemed that, thanks to the slotting, the blockage is negligible, no direct confirmation of that is offered in Ref. 1. Also, as mentioned in the Introduction, fair agreement between two-dimensional CFD and the data¹ has, as a rule, been reached by quite a tangible alteration of the angle of attack. This suggests that the difference between free air CFD and slotted floor and ceiling conditions is serious.

These considerations first led us to perform a study of turbulence-model sensitivity for case 10, followed by computations in a range of the freestream parameters (M and α).

Effect of Turbulence Model

Two turbulence models besides S-A, the SARC and M-SST models, have been used. This choice seems quite justified. The SARC model has at least potential advantages over the original S-A model, particularly for three-dimensional flows, and the M-SST model is commonly considered one of the best (if not the best) two-equation model for flows with shock-induced separation.

A comparison of the three models' performance in the two-dimensional and three-dimensional setups is shown in Fig. 8, where we present their predictions of the pressure distribution at the airfoil symmetry plane and, also, in Table 1 (runs 1–3 and 11–13, respectively). First, note that in three-dimensional mode, the difference between the S-A and SARC models is negligible in that plane, whereas the M-SST prediction is quite a bit worse. This behavior is quite different from that observed in the two-dimensional RANS solutions

with an adjusted angle of attack (see, for example, Ref. 4) where the M-SST model fares somewhat better than the S-A one, as well as differing from what our two-dimensional computations give at the nominal angle of attack. (See Fig. 8 and Table 1.) Therefore, the ratings of the models turn out to be significantly dependent on whether a two-dimensional or three-dimensional problem statement is used. Also, whichever the model, the three-dimensional predictions of the pressure distribution and integral lift and drag remain rather poor.

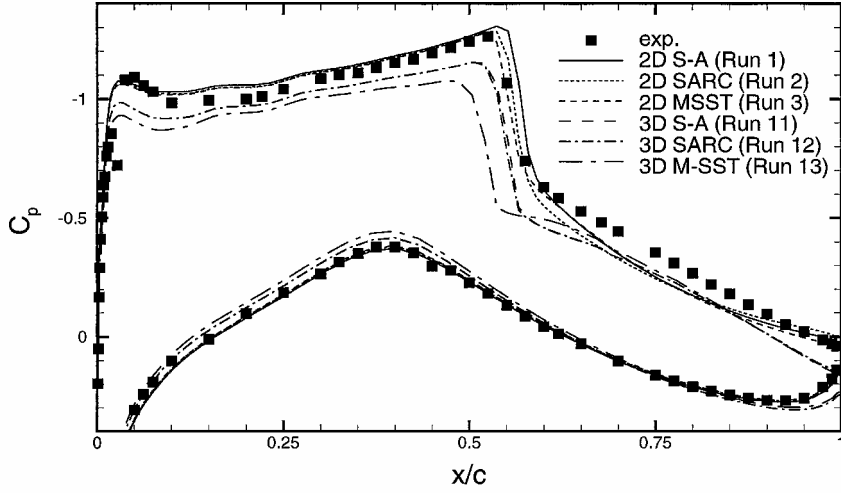
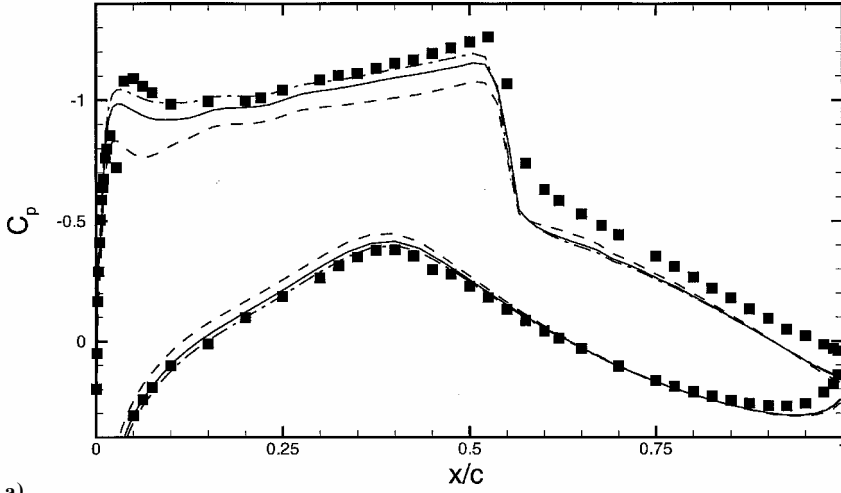


Fig. 8 Effect of the turbulence model on the pressure coefficient streamwise distribution at the airfoil symmetry plane for the experimental flow regime case 10.



a)

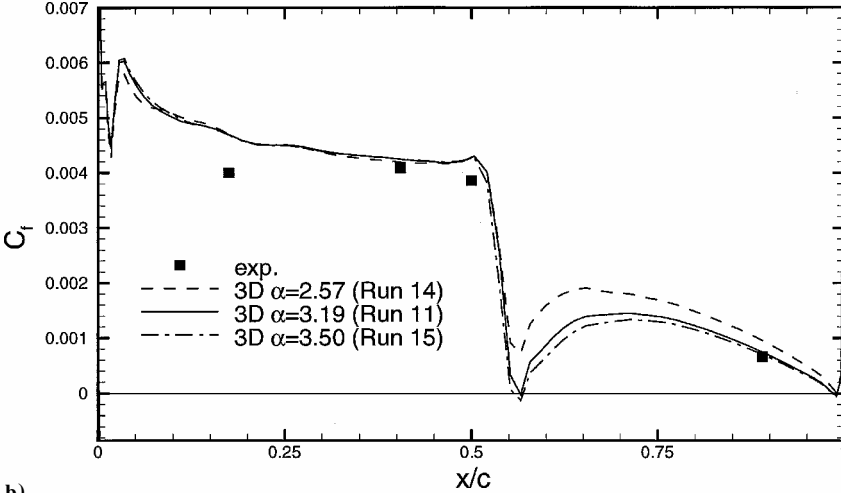


Fig. 9 Effect of the angle of attack on a) the pressure and b) friction coefficients streamwise distribution at the airfoil symmetry plane for the experimental flow regime case 10.

For instance, the difference between the computed and measured lift coefficients C_L at the symmetry plane of the airfoil ranges from 12 to 19%, depending on the model being used. (Compare runs 11–13.) This suggests that, at least partially, the discrepancy is caused not by the flaws of the turbulence models, but by an inadequate representation of the experimental setup and, first, by not accounting for the floor and ceiling of the test section. To check this conjecture, following a practice common in two-dimensional studies, we performed computations with different values of the flow freestream Mach number and angle of attack. In addition to that, one case was computed at the nominal values of those parameters but with both side walls and a nonslotted floor and ceiling of the test section. The latter run is aimed at evaluating the maximum possible effect of the floor and ceiling in the experiments.

Effect of Freestream Parameters and of Floor and Ceiling of the Test Section

The study includes variation of α in the range from 2.57 to 3.5 deg. (Recall that the experimental value of α considered in all of the preceding computations is 3.19 deg.) The freestream Mach number also varies, in the range from 0.73 to 0.77 (experimental value, 0.75). The results obtained in this series are shown in Figs. 9 and 10.

First of all, the effect of α (Fig. 9) turns out to be qualitatively different in the three-dimensional (with side wall) and two-dimensional computations. In three dimensions, variation of α results in quite noticeable changes of the pressure distribution upstream of the shock and of its intensity, but it leaves the shock position and postshock pressure distribution at the airfoil symmetry plane almost unaf-

fected. Recall that, in two dimensions, the increase of α causes a significant pressure alteration almost everywhere and, in particular, results in a tangible downstream shift of the shock. (The two-dimensional pressure distributions are not shown for clarity but are consistent with the literature and are reflected by the lift in Table 1.) As far as the skin friction is concerned, both three-dimensional and two-dimensional predictions upstream of the shock are almost insensitive to α variations in the considered range. Downstream of the shock, the reaction of the skin friction to α is similar to that of the pressure and reflects the change of the intensity of the shock in the three-dimensional computation and its shift downstream in the two-dimensional computation. Unlike the two-dimensional result, the three-dimensional solutions reattach after the shock, in agreement with the single experimental point.

Second, as is clearly seen in Table 1, to get the experimental lift in the framework of the three-dimensional (with account of side walls) RANS, one needs to increase α . (Even at $\alpha = 3.5$ deg, the computed value of C_L is still quite a bit lower than in the experiment.) On the other hand, in the framework of the two-dimensional RANS, to get the experimental lift, α should be decreased relative to the experimental value. This means that, in contrast to the two-dimensional computations, in the three-dimensional ones there is no chance of getting good agreement with the experiment on both lift and drag at any α .

Quite a similar picture is observed when the freestream Mach number is varied (Fig. 10). The reaction of the three-dimensional and two-dimensional pressure and skin-friction distributions and of the integral forces to M variations are quite different. For the

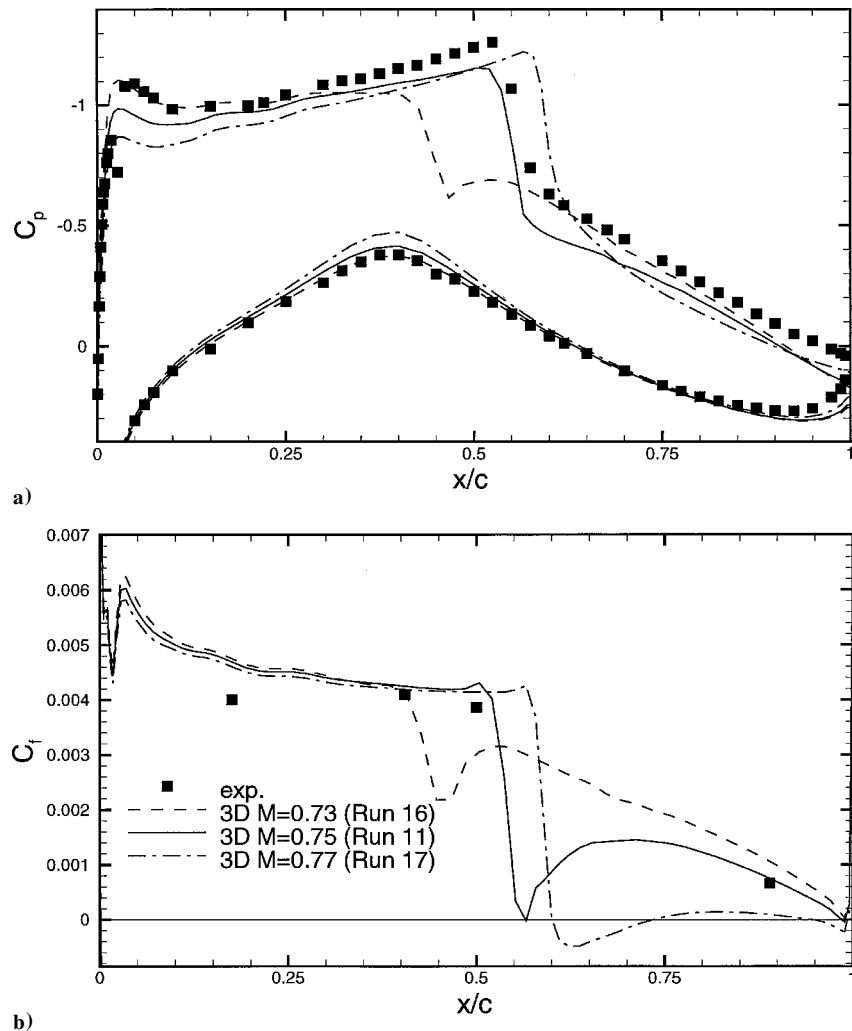


Fig. 10 Effect of the Mach number on a) the pressure and b) friction coefficients streamwise distribution at the airfoil symmetry plane for the experimental flow regime case 10.

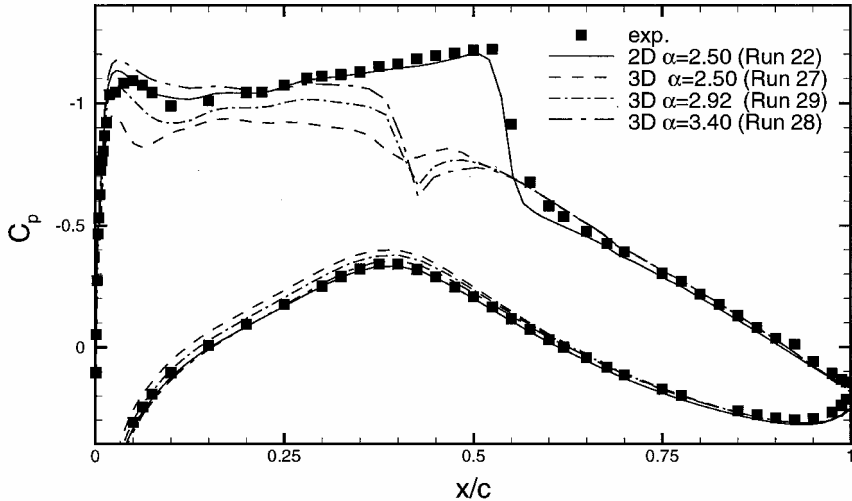


Fig. 11 Effect of the angle of attack on the pressure coefficient streamwise distribution at the airfoil symmetry plane for the experimental flow regime case 6.

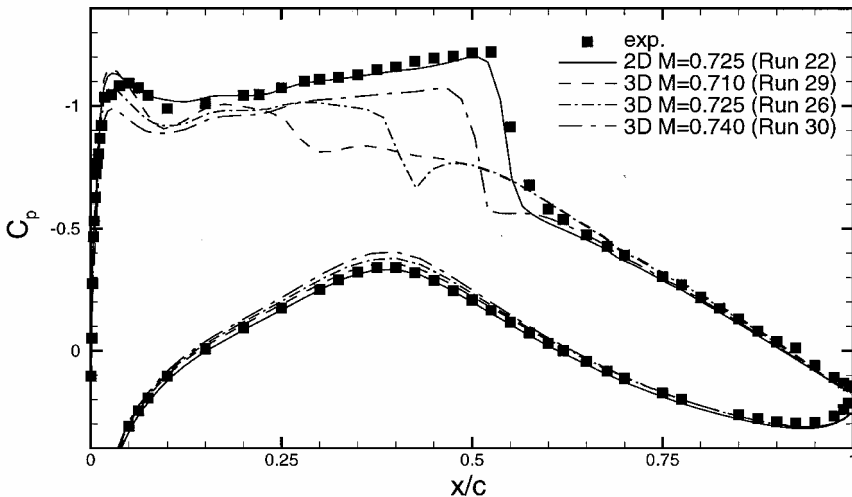


Fig. 12 Effect of Mach number on the pressure coefficient streamwise distribution at the airfoil symmetry plane for the experimental flow regime case 6.

three-dimensional case, deviations of the Mach number from the experimental value of 0.75 do not provide any global improvement of the predictions.

The general conclusion can be made on the basis of the preceding observations that the relative success of the freestream parameter adjustment procedure in two-dimensional RANS is, most probably, just a result of cancellation of the errors caused by the use of the two-dimensional approach without adequate account of the effect of the wind-tunnel walls.

It could be expected that the preceding issues might be less severe for case 6 ($\alpha = 2.92$ deg and $M = 0.725$), which is commonly considered an easier test for the two-dimensional RANS due to the absence of separation. However, this turns out not to be true. As seen in Figs. 11 and 12 and in Table 1 (cases 22–25 and 27–30), qualitatively, the difference between the two-dimensional and three-dimensional predictions for this flow is the same as that for case 10, but is even more pronounced. This is probably caused by a stronger effect of the side walls on the central part of this flow due to a weaker shock. In each case we showed only the two-dimensional case with optimized angle of attack, $\alpha = 2.5$ deg.

Thus, the results obtained show that the procedure of adjusting the freestream parameters in the framework of two-dimensional RANS routinely used for evaluation of the capabilities of turbulence models, at least as far as the RAE 2822 flow is concerned, is not justified. The only way to obtain objective data on those capabilities is to reproduce all of the details of the experimental setup.

As a first step in this direction, we performed a three-dimensional computation of case 10 with account taken of not only the side walls, but also of the nonslotted floor and ceiling. The expectation was that the predictions would move from those accounting only for side walls toward the experimental data, possibly moving too far. This expectation was met only partially. This is seen in Fig. 13, where we compare two two-dimensional and two three-dimensional solutions. As expected, the experimental shock position does lie between the two predictions. However, upstream and downstream of the shock, especially, in the regions $x < \sim 0.25$ and $x > \sim 0.75$, the pressure distributions computed with and without account taken of the floor and ceiling are very close to each other.

Possible reasons for that disagreement, other than turbulence-model deficiencies, might be a nonlinear interaction of the slotted floor and ceiling and the side walls. Unfortunately, it is difficult to check that by a direct computation, due to the lack of data on the ambient parameters in the experiment. However, whatever the reasons are, one thing seems to be clear: Available experimental data on transonic airfoils are insufficient to make definite conclusions about RANS turbulence models' capabilities. Moreover, based on the study outlined from the standpoint of turbulence model validation, trying to reach strictly two-dimensional conditions in the experiments is less productive than planning and ensuring the reproducibility of a real three-dimensional experimental setup in three-dimensional CFD. The world has changed since the RAE study was conducted, around 1978.

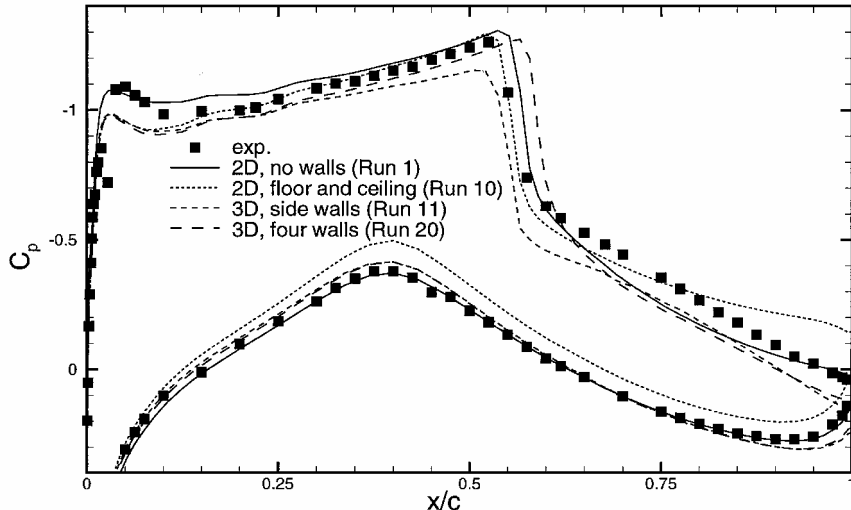


Fig. 13 Effect of the walls of the test section on the pressure coefficient streamwise distribution at the airfoil symmetry plane for the experimental flow regime case 10.

Conclusions

An extensive RANS study was performed of the three-dimensional effects associated with the walls of the test section of the wind tunnel in the experiments with the RAE 2822 transonic airfoil. A major conclusion that can be drawn on the basis of the results obtained is that the conventional two-dimensional approach to modeling such flows is, most probably, incorrect and may even result in an incorrect assessment of turbulence models' capabilities. Furthermore, the available experimental data on transonic airfoils are insufficient from the standpoint of turbulence-model validation because they do not allow us to reproduce all of the relevant details of the experimental setup in three-dimensional CFD. Slotted walls are particularly troublesome; they are helpful for testing airplane designs, not for CFD and model validation. An aspect ratio equal to 3 is insufficient and is far from justified by the Reynolds number gain it allows. Jiang's⁹ findings for an experiment with side-wall suction also indicate that such suction fails to resolve the side-wall issue. These findings illustrate again the value of axisymmetric experiments, short of experiments conducted on complete wings. They also show that computer power, even at the personal computer level as in this study, has resolved the conundrum of creating data sets that are two-dimensional and free of any wall effects for CFD validation; this is simply not necessary anymore.

Acknowledgments

The work was supported by the Boeing Technology Research Center in Moscow. We are grateful to L. Wigton for providing the two-dimensional grid for the airfoil.

References

- ¹Cook, P. H., McDonald, M. A., and Firmin, M. C. P., "Aerofoil RAE 2822—Pressure Distributions and Boundary Layer and Wake Measure-

ments," AR 138, AGARD, 1979, pp. A6-1–A6-77.

²Spalart, P. R., and Allmaras, S. R., "A One-Equation Turbulence Model for Aerodynamic Flows," *La Recherche Aérospatiale*, No. 1, 1994, pp. 5–21.

³Hellstrom, T., Davidson, L., and Rizzi, A., "Reynolds Stress Transport Modelling of Transonic Flow Around the RAE2822 Airfoil," AIAA Paper 94-0309, Jan. 1994.

⁴Shur, M. L., Strelets, M. Kh., Travin, A. K., and Zaikov, L., "Comparative Study of One- and Two-Equation Turbulence Models for Incompressible and Transonic Flows with Separation and Reattachment," *Engineering Turbulence Modelling and Experiments 3*, edited by W. Rodi and G. Bergeles, Elsevier, New York, 1996, pp. 697–706.

⁵Haase, W., Brandsma, E. F., Leschziner, M., and Schwamborn, D. (eds.), "EUROVAL—A European Initiative on Validation of CFD-Codes," *Notes on Numerical Fluid Mechanics*, Vieweg, Brunswick, Germany, 1993, Sec. 5.1, pp. 125–185.

⁶Vos, J. B., "Activity Report Thematic Area External Aerodynamics," *QNET-CFD Network Bulletin*, No. 1, Jan. 2001, pp. 9–11.

⁷Menter, F. R., "Two-Equation Eddy-Viscosity Turbulence Models for Engineering Applications," *AIAA Journal*, Vol. 32, No. 8, 1994, pp. 1598–1605.

⁸Spalart, P. R., "Trends in Turbulence Treatments," AIAA Paper 2000-2306, June 2000.

⁹Jiang, F., "CFD Predictions for Control Surface Effectiveness," AIAA Paper 2000-0510, Jan. 2000.

¹⁰Spalart, P. R., and Shur, M. L., "On the Sensitization of Turbulence Models to Rotation and Curvature," *Aerospace Science and Technology*, Vol. 1, No. 5, 1997, pp. 297–302.

¹¹Roe, P. L., "Approximate Riemann Solvers, Parametric Vectors and Difference Schemes," *Journal of Computational Physics*, Vol. 43, 1981, pp. 357–372.

P. Givi
Associate Editor